Surface Induced Dissociation Yields Quaternary Substructure of Refractory Noncovalent Phosphorylase B and Glutamate Dehydrogenase Complexes

ARTICLE *in* JOURNAL OF THE AMERICAN SOCIETY FOR MASS SPECTROMETRY · JANUARY 2014

Impact Factor: 2.95 · DOI: 10.1007/s13361-013-0790-y · Source: PubMed

3 AUTHORS, INCLUDING:

Mowei Zhou
Pacific Northwest National Laboratory
14 PUBLICATIONS **133** CITATIONS

J. Am. Soc. Mass Spectrom. (2014) 25:368–379
DOI: 10.1007/s13361-013-0790-y

RESEARCH ARTICLE

Surface Induced Dissociation Yields Quaternary Substructure of Refractory Noncovalent Phosphorylase B and Glutamate Dehydrogenase Complexes

Xin Ma, Mowei Zhou, Vicki H. Wysocki

Department of Chemistry and Biochemistry, The Ohio State University, 876 Biological Sciences Building, 484 W 12th Ave, Columbus, OH 43210, USA

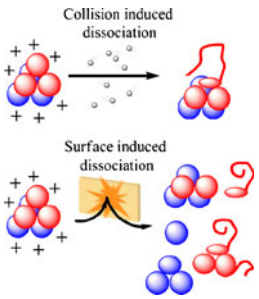

Abstract. Ion mobility (IM) and tandem mass spectrometry (MS/MS) coupled with native MS are useful for studying noncovalent protein complexes. Collision induced dissociation (CID) is the most common MS/MS dissociation method. However, some protein complexes, including glycogen phosphorylase B kinase (PHB) and L-glutamate dehydrogenase (GDH) examined in this study, are resistant to dissociation by CID at the maximum collision energy available in the instrument. Surface induced dissociation (SID) was applied to dissociate the two refractory protein complexes. Different charge state precursor ions of the two complexes were examined by CID and SID. The PHB dimer was successfully dissociated to monomers and the GDH hexamer formed trimeric subcomplexes that are informative of its quaternary structure. The unfolding of the precursor and the percentages of the distinct products suggest that the dissociation pathways vary for different charge states. The precursors at lower charge states (+21 for PHB dimer and +27 for GDH hexamer) produce a higher percentage of folded fragments and dissociate more symmetrically than the precusors at higher charge states (+29 for PHB dimer and +39 for GDH hexamer). The precursors at lower charge state may be more native-like than the higher charge state because a higher percentage of folded fragments and a lower percentage of highly charged unfolded fragments are detected. The combination of SID and charge reduction is shown to be a powerful tool for quaternary structure analysis of refractory noncovalent protein complexes, as illustrated by the data for PHB dimer and GDH hexamer.

Key words: Surface induced dissociation, Tandem mass spectrometry, Quaternary structure, Protein complex, Charge state, Ion mobility, Nanoelectrospray

Received: 16 September 2013/Revised: 11 November 2013/Accepted: 19 November 2013/Published online: 23 January 2014

Introduction

Native mass spectrometry (native MS) is a method to study stoichiometry, structure, and intermolecular interactions of noncovalent protein assemblies [1–6]. The intact protein complexes are ionized by nano-electrospray ionization (nano-ESI) under gentle interface conditions and analyzed directly by MS [1–6]. There is plenty of evidence to support that protein assemblies can be intact and folded in vacuum [1–8]. Native MS is a versatile and robust technique and even mega-Dalton range virus capsids have been successfully analyzed [9–12]. Native MS can be coupled with ion mobility (IM) and tandem mass spectrometry (MS/MS) to provide additional information about the conformations of protein complexes [1–5, 7, 8, 13–16].

Briefly, IM is a technique where ions are driven by an electric field through a drift tube filled with bath gas to separate ions with different charge states, sizes, and shapes. Under the acceleration of electric fields, ions with larger collision cross sections (CCS) and lower charge states migrate slower in the drift tube [13–17]. By coupling IM with MS, ions with the same mass-to-charge ratio (m/z) but different shapes can be separated by IM because they have different drift times [13–16]. To reveal the potential structures of the analyte, the theoretical CCSs of structures based on X-ray crystallography, nuclear magnetic resonance (NMR), molecular dynamics simulations or even coarse

Electronic supplementary material The online version of this article (doi:10.1007/s13361-013-0790-y) contains supplementary material, which is available to authorized users.

Correspondence to: Vicki H. Wysocki; *e-mail:* wysocki.11@osu.edu

grain models can be calculated to compare with the experimental CCS [11, 13–15, 18, 19].

MS/MS is employed to isolate and dissociate protein assemblies to reveal the numbers and identities of the subunits. The most common commercial activation method is collision induced dissociation (CID). Other activation methods, including blackbody infrared radiative dissociation (BIRD), electron-capture dissociation (ECD), infrared and ultraviolet multiphoton dissociation (IRMPD and UVPD) and surface induced dissociation (SID), can also be used [2, 3, 5, 6, 20–22]. In typical CID, energy is deposited into the ions by multiple low-energy collisions. In contrast, SID deposits energy into the ions in a faster time scale by a single collision event with a surface [23–26]. Typical CID fragmentation of protein complexes is through charge "assymmetric" pathways producing highly charged monomers and complementary (n-1)-mers [26–30] because unfolding [27, 28, 30] and charge enrichment [27] of the monomer are involved in the dissociation process. Alternative dissociation pathways have been reported in charge-reduced [30] and supercharged protein complexes [31, 32], where folded monomers and subcomplexes [30–33] could be observed in CID. The findings highlight manipulation of charge states as a means to reveal more structural information by CID. SID was previously applied to several protein complexes and provided a more "symmetric" or proportional dissociation pattern (relatively equal distribution of charges and not dominant unfolded monomer fragments) than CID [23–26, 34–36]. Also, more or alternative dissociation pathways are observed in SID because the rapid [26] high energy input with a much more massive target can lead to dissociation into compact subunits [23–26]. Recent studies that used SID coupled to IM-MS for several tetrameric and pentameric proteins illustrated that most SID products are compact [37–39]. In addition, SID produces a wide variety of products from GroEL tetradecamer, including heptameric products indicative of the "ring on ring" structure [40]. The fragmentation patterns of SID show that it is an informative activation method that is complementary to CID in large protein complex analysis.

Previous studies of individual small biomolecules or proteins generated from denaturing solutions have shown that the conformations of different charge states may vary, and the CCSs of lower charge states are more similar to the native state CCS [8, 19, 41–44]. One explanation for this is that lower charge state ions have weaker Coulombic repulsion, thus preserving their native-like structure [19, 42–44]. It is not clear whether lower charge states guarantee native conformations for larger protein complexes generated from buffered aqueous solutions. The unfolding and dissociation of protein complexes can be charge-dependent processes for both CID [30, 31] and SID [39]. At reduced charge states, CID produces less extensive precursor dissociation than at higher charge states at the same collision energy. However, extensive dissociation of noncovalent protein complexes into subunit products can be observed in SID of complexes at reduced charge states. With better preservation of subunit contact information from charge-reduced precursors [39], charge reduction could provide more information to explore the structure of native-like protein complexes [30, 39].

Two protein complexes that are resistant to dissociation by CID were selected for this study to further reveal the potential of SID in protein complex structure elucidation. Both glycogen phosphorylase B kinase (PHB) and L-glutamate dehydrogenase (GDH) do not dissociate significantly in CID for the two charge states examined even at the maximum collision energy available in the instrument. SID successfully dissociates both of them, with unfolded and folded fragments observed. Triethylammonium acetate (TEAA) added to ammonium acetate was used to reduce the charge states for comparing SID fragmentation behaviors of different charge states [39]. Different SID voltages were applied to systematically study the dissociation pathways and the dissociation pathways of different charge states of the protein complexes are proposed.

Experimental

Protein Preparation

PHB from rabbit muscle, GDH from bovine liver, transthyretin (TTR), and concanavalin A (ConA) were purchased from Sigma-Aldrich (St. Louis, MO, USA). Serum amyloid P (SAP) was purchased from EMD Millipore Corporation (Chicago, IL, USA). The protein powders were dissolved in deionized water to 50–100 μM and buffer exchanged into 100 mM ammonium acetate (Sigma-Aldrich, St. Louis, MO, USA) at pH 7, with Micro Bio-Spin 6 chromatography columns (Bio-Rad Laboratories, Inc., Hercules, CA, USA). The final monomer protein concentrations of TTR, ConA, SAP, and PHB were 50 μM, and that of GDH was 100 μM. Triethylammonium acetate (TEAA) was purchased from Sigma-Aldrich (St. Louis, MO, USA) at pH 7 and added into the protein solutions to achieve 0.1/0.9 TEAA/ammonium acetate (vol/vol) for charge reducing experiments as indicated in the text (higher concentration of TEAA does not further reduce the charge state).

Ion Mobility-Mass Spectrometry (IM-MS) with Surface Induced Dissociation (SID)

IM-MS was performed on a Synapt G2 HDMS (Waters MS Technologies, Manchester, UK) [45, 46] modified to include a custom SID device [38]. The SID device is located before the IM cell as described previously [38] in order to record the drift time of the SID fragments. Ions are accelerated in SID experiments by increasing "Trap DC Bias," which increases all the DC offsets on the Trap cell and upstream of the Trap cell, and the ion beam is steered toward the surface for SID by controlling the voltages on the surface and lenses in the device. SID MS/MS was performed over a range of

acceleration voltages from 30 to 190 V at 10 V increments. When recording MS and CID spectra, the voltages of the SID device are set to transmit the ions through without hitting the surface. All CID was performed in the Trap cell.

In nano-ESI, each sample is loaded into a tapered glass capillary (inner diameter of the non-tapered end is 1 mm) pulled in-house using a Sutter Instruments P-97 micropipette puller (Novato, CA). A platinum wire is inserted into the non-tapered end of the capillary and a voltage of 1.2–1.5 kV is applied. The cone voltage was optimized at 50 V and the ion source temperature was ~30 °C to minimize denaturation of protein complexes. Pressure in the source region was raised to about 6 mbar by partially restricting the vacuum line to the rotary pump to optimize ion collisional cooling and transmission.

All samples were analyzed with argon as the collision gas and nitrogen as the ion mobility gas. The pressure reading of argon in the transfer ion guide was ~1.2×10^{-2} mbar. The pressure reading of argon in the trap was 3.3×10^{-2} mbar for most experiments but was 4.6×10^{-2} mbar for trap CID of GDH. CID MS/MS was performed over a range of collision voltages from 20 to 200 V in the trap collision cell at 10 V increments. For better transmission in the trap collision cell, the lowest collision voltage was set to 20 V and the CCSs do not change at lower collision voltages. The flow rate to the helium cell, which is used for collisional cooling of ions before they enter the IM chamber [46], was 120 mL/min. The pressure of nitrogen in the ion mobility cell was 2.2 mbar. The ion mobility spectrometry (IMS) wave height and velocity were varied at (16.0 V, 300 ms^{-1}), (16.0 V, 280 ms^{-1}), (16.0 V, 260 ms^{-1}) for PHB dimer at +29, (20.0 V, 240 ms^{-1}), (18.0 V, 220 ms^{-1}), (16.0 V, 200 ms^{-1}) for PHB dimer at +21, and (22.0 V, 240 ms^{-1}), (21.0 V, 220 ms^{-1}) and (20.0 V, 200 ms^{-1}) for GDH hexamers at +39 and +27. The experiments were repeated under different wave heights and velocities to evaluate variation of CCSs and percentages of SID fragments and were optimized based on the literature [13, 47, 48] and research group experience with large complexes. The time-of-flight (TOF) analyzer pressure was 7.0×10^{-7} mbar.

To normalize the contribution of different charge states to collision energy, the laboratory frame collision energy (E_{lab}) was used. E_{lab} is defined as:

$$E_{lab} = V_{acceleration} \times z$$

where $V_{acceleration}$ in the equation represents the acceleration voltage of CID or SID, and z represents the nominal charge state of the selected ion.

Collision Cross Section (CCS) Calibration and Calculation

Calibration of the CCS was performed following the protocol of references [49, 50] with TTR tetramer, ConA tetramer, SAP pentamer, SAP decamer, and GDH hexamer as the calibration standards [50]. All mass spectra were analyzed by MassLynx ver. 4.1 and all mobiligrams were analyzed using DriftScope ver. 2.4 provided by Waters MS Technologies (Manchester, UK).

The Jarrold group has developed an open source software program—MOBCAL—to calculate helium based CCSs of molecules [51, 52]. MOBCAL was used to calculate the projection approximation (PA) using models prepared from X-ray crystallographic structures [13, 19, 51, 52]. Theoretical CCSs were calculated with the scaled PA method developed by the Robinson group [31, 53]. The file 8GPB.pdb [54] was used for PHB monomer CCS calculation and 3MVO.pdb [55] was used for GDH monomer and trimer CCS calculations. Chain A in the 8GPB.pdb was extracted to represent PHB monomer. Chain A in the 3MVO.pdb was extracted to represent GDH monomer, and Chain A, B, and C were extracted to represent GDH trimer. Chain extraction and addition of hydrogen were completed with the PyMOL Molecular Graphics System, ver. 1.5.0.4 Schrödinger, LLC. Computations of CCSs with MOBCAL were performed on a 2.66 GHz Xeon Westmere-EP Dual 6-core (Santa Clara, CA, USA) server at the University of Arizona High Performance Computing Service.

Results and Discussion

Glycogen Phosphorylase B Kinase (PHB) Dimer Dissociates in Surface Induced Dissociation (SID) But Not in Collision Induced Dissociation (CID)

PHB is a dimer of two identical 97.2 kDa monomers [54, 56–61]. Its structure is well studied and its X-ray crystal structure is available [54], making it a suitable model for fragmentation studies. The +29 and +21 were among the most abundant dimer peaks in the mass spectra of PHB in ammonium acetate and PHB in ammonium acetate plus TEAA, respectively (Supplementary Figure S-1). Odd charge number precursor ions (PHB dimer at +29 and +21 in this study) were selected because the *m/z* of the precursor does not overlap with those of the products, thus eliminating interference from products to the precursor CCS measurement. CID was first employed to attempt to dissociate the complex. The dimer at +29 did not dissociate significantly at an acceleration voltage 200 V, which is the highest acceleration voltage of the instrument (Figure 1a), although a small number of charge stripping peak (+28 precursor) was observed. Similarly, the lower charge state (+21) dimer did not dissociate by CID either (Figure 1b), but it showed a charge stripping peak (+20 precursor). The dimer is, therefore, a refractory protein complex in the gas phase, with MS/MS by CID difficult. CCS changes at different CID E_{lab} reveal that the selected dimers (+29 and +21) are energized by the collision because the dimers unfold, or collapse and then unfold, in CID (Supplementary Figure S-2) and the +29 and +21 unfolding behaviors are different, which is

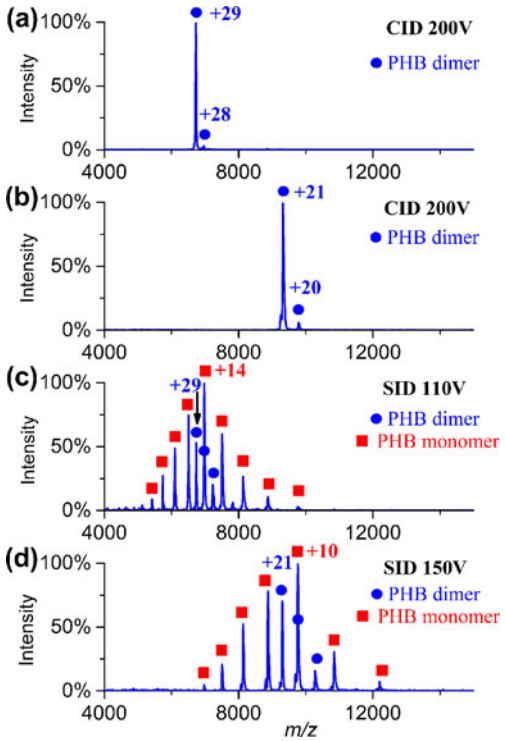

Figure 1. CID and SID spectra of PHB dimer at +29 and +21. (**a**) PHB dimer at +29 does not dissociate significantly in CID at 200 V acceleration voltage, which is the maximum accessible voltage in the instrument. No monomer is produced. (**b**) PHB dimer at +21 does not dissociate in CID at 200 V either. (**c**) PHB dimer at +29 dissociates to monomer at 110 V SID acceleration voltage (3190 eV). The charge states of the monomers are centered at around half of the charge state of the dimer. Such a symmetric dissociation is consistent with our previous SID results for some other proteins. (**d**) PHB dimer at +21 dissociates to monomer at 150 V SID acceleration voltage (3150 eV). SID produces symmetric dissociation and the E_{lab} of (**c**) and (**d**) are similar, at 3190 and 3150 eV, respectively

in agreement with previous research showing different unfolding pathways of different charge states [8, 30, 31, 39].

The dimer at +29 has two distinct conformational states (Supplementary Figure S-2a and b). The CCS increased to ~100 nm^2 and then further increased to ~130 nm^2 at 3200 eV and did not increase any more even at the highest acceleration voltage. Although the CCS of dimer at +21 is similar to +29 without significant activation, it decreased slightly to ~85 nm^2 and increased abruptly to ~100 nm^2 at E_{lab} 3000 eV (Supplementary Figure S-2c and d), with evidence of another conformer just beginning to emerge at the highest collision energy. We suspect that the different unfolding pathways may come from different distributions of charges on the protein surface because the charges and their migration are involved in unfolding [28, 31, 62]. Neither the unfolded nor collapsed PHB dimer dissociate in CID. Because CID deposits energy into the precursor stepwise, low energy barrier pathways are preferred [23–26].

To further study the higher energy dissociation pathways that might provide more quaternary structural information, SID was applied to the precursors. PHB dimers at both +29 and +21 dissociate into monomers in SID (Figure 1c and d). The charge states of the monomers are centered at around half of the charge state of the precursor, showing a "symmetric" dissociation pattern. The CCSs of the monomers at various charge states are shown in Figure 2. The CCSs of the lower charge state monomers (≤13) from different precursors are similar. The CCS of the +14 monomer from +21 precursor is larger than that from +29 precursor, implying that they may have formed through different pathways attributable to different precursor charging patterns or conformations. The CCSs of the monomers above +15 (from the +29 precursor) or +14 (from the +21 precursor) become increasingly larger with increasing charge state. Additionally, the CCSs are significantly larger than those of the lower charge states, indicating that higher charge states must be partially unfolded monomers. The CCSs of the folded monomers are close to the calculated result, indicating the monomer's native-like structure can be preserved in SID.

In order to probe the energy barriers of the dissociation pathways, the unfolding of the unfragmented precursors and the percentages of precursors and fragments were monitored across a range of SID acceleration voltages from 30 V to 190 V (Figure 3). These are currently the lowest and highest SID acceleration voltages accessible, respectively. The

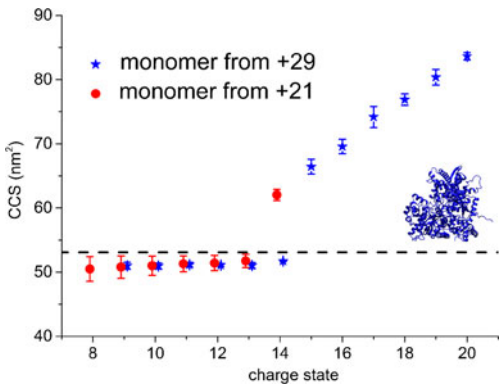

Figure 2. CCSs of different charge states of PHB monomer in SID. Blue filled stars represent CCSs of monomers from PHB dimer at +29. Red filled circles represent CCSs of monomers from PHB dimer at +21. The CCSs of +9 to +13 monomers from different precursors are similar. The CCS of the +14 monomer from +21 precursor is larger than that from +29. When the charge state is higher than 15, the CCS increase with charge state shows that higher (≥15 for monomer from +29 precursor and ≥14 for monomer from +21 precursor) charge state monomers are unfolded. The dashed line shows the calculated CCS of the PHB monomer clipped from the dimer crystal structure. Symbols are slightly displaced to more clearly illustrate overlapping points. The variation of measured CCSs at three different wave volecities and wave heights (refer to Experimental) are represented by the error bars

percentages of fragments and unfragmented precursors are determined by dividing the total peak area of a given species at all of its charge states by the total peak area of all the species in the spectrum after background subtraction. The SID spectra and CCS distributions of remaining precursors in SID at different E_{lab} are included in Supplementary Figures S-3 and S-4. The CCS of the +29 precursor (Figure 3a) is ~100 nm^2 at SID E_{lab} 870 eV (acceleration voltage 30 V), however, the CCS of the precursor at the lowest CID E_{lab} (20 V collision voltage) is only 90 nm^2 (Supplementary Figure S-2), indicating the precursor has slightly expanded or partially unfolded at the lowest SID acceleration voltage in the experiment. The percentage of the folded monomer at E_{lab} 870 eV is 15 % (Figure 3b), but whether the precursor needs to expand or partially unfold to produce the folded monomer is unclear. Very little unfolded monomer from +29 precursor is observed when the E_{lab} is 870 eV (Figure 3b), suggesting that expansion better explains the slightly higher CCS than partially unfolding. When the E_{lab} is higher, the unfragmented +29 precursor unfolds rapidly and reaches ~140 nm^2 at E_{lab} 2500 eV (Figure 3a). The percentage of unfolded monomer increases rapidly to about 40 % in the same E_{lab} range (Figure 3b), supporting the hypothesis that formation of unfolded monomer requires unfolding of the precursor. The percentages of the dimer, folded monomer, unfolded monomer, and the CCS of the unfragmented precursor do not change greatly at E_{lab} above 2500 eV (Figure 3a and b).

In contrast to the +29, the PHB dimer precursor at +21 starts to unfold or expand (Figure 3c and Supplementary Figure S-4b) and produces folded monomer only when SID E_{lab} is about 1200 eV and the folded monomer is the major product in the dissociation (Figure 3d). In CID, the CCS of the +21 precursor decreases when the collision energy increases (Supplementary Figure S-2b). In contrast, CCS of the +21 precursor does not descrease in SID, indicating the precursor unfolding pathway of SID is different from that observed in CID. The CCS of the unfragmented precursor (Figure 3d) plateaus at E_{lab} higher than 2000 eV although the monomer/precursor ratios continue to change slightly. The percentage of the unfolded monomer increases slowly in the E_{lab} range of the experiment and is no higher than 10 % even at 4000 eV (Figure 3d). The increase of unfolded monomer is consistent with an additional decrease in precursor intensity, greater than what can be accounted for by only the slight change in folded monomer.

It is noteworthy that the percentage of the folded monomer from the +29 dimer is stable in the E_{lab} range of this expeimrent (Figure 3b). Even at the lowest SID E_{lab}, the percentage of the folded monomer is 18 %. Also, the charge distribution of monomer does not change significantly at different SID E_{lab} (Supplementary Figure S-3a–d). We hypothesize there might be a population of +29 dimer with initial conformations that easily dissociate into folded monomers. Although the CCSs of +29 and +21 dimers at the lowest CID E_{lab} are similar (Supplementary Figure S-2),

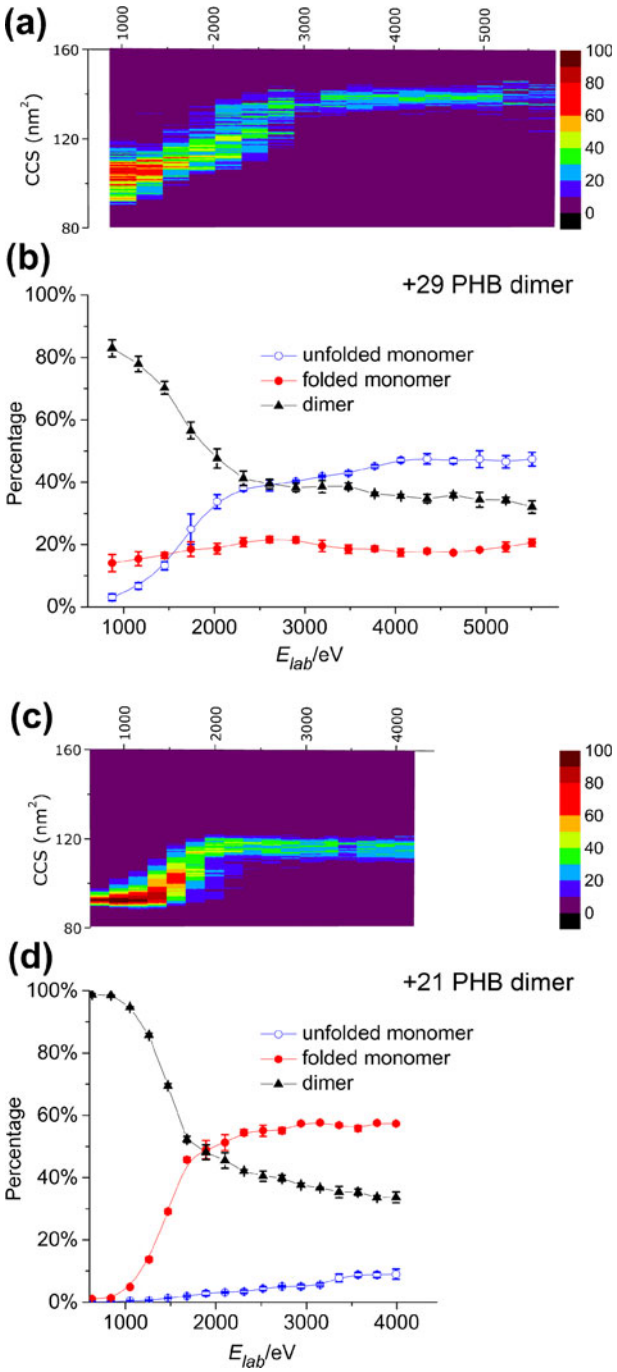

Figure 3. (**a**) Precursor CCSs of PHB dimer at +29. The intensity is normalized to the percentage of the unfragmented dimer. The CCS of the unfragmented dimer icreases when E_{lab} increases. (**b**) Percentages of different species. Unfolded monomer becomes the major fragment when E_{lab} is higher than 1700 eV. (**c**) Precursor CCSs of PHB dimer at +21. The intensity is normalized to the percentage of the unfragmented dimer. The CCS of the unfragmented dimer begins to increase at 1300 eV and reaches ~120 nm^2 when E_{lab} is above 1800 eV. (**d**) Percentages of different species. Folded monomer is the major fragment across the E_{lab} range. All four plots are aligned in the E_{lab} axis for direct comparison of collision energies. The experiments were performed three times at different wave velocities and wave heights, with the variation of the results marked by the error bars

the +29 dimer has a full width at half maximum (FWHM) of 7 nm^2, remarkably larger than that of the +21 dimer (4 nm^2). The broader CCS distribution of the +29 implies that there are more possible conformational states contributing than for the +21 dimer, despite the insufficient IM resolution to resolve them. The additional conformational states may originate from preactivation in the ion source, and/or variability in charge distributions on the protein surface. It has been reported that charge partitioning and migration are important factors in the unfolding process [28, 31, 62]. In addition, theoretical calculation of protonated cytochrome *c* dimer indicates that the complex with symmetric charge partitioning tends to produce monomers with little structural change, whereas the complex with asymmetric charge partitioning preferentially produces unfolded, higher charged monomers [63–65]. Thus, we speculate that the dimers with different charge distributions could each undergo a different dissociation pathway, giving rise to the different behavior in the breakdown curve (Figure 3b).

To summarize and explain the observations for SID fragmentation of PHB dimer at +29 and +21, hypothetical, simplified dissociation pathways are proposed in Scheme 1. Because the precursor at +29 had expanded or unfolded under the lowerest SID E_{lab}, it is not clear whether the folded monomer is directly dissociated from the folded precursor. Because the percentage of folded monomer is

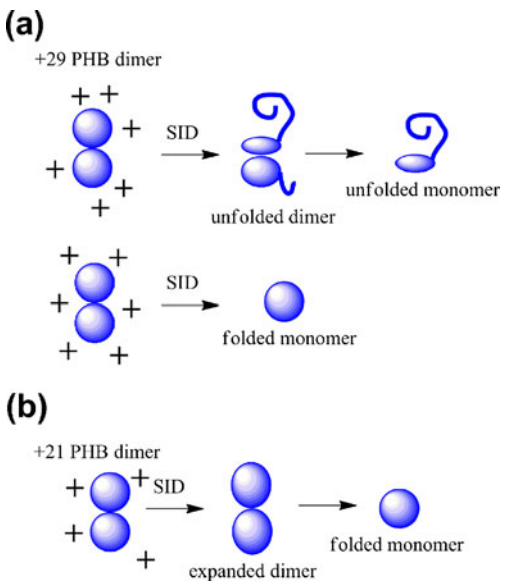

Scheme 1. (**a**) The hypothetical, simplified dissociation pathway of PHB dimer at +29. The dimer can dissociate to folded monomer, or unfold, and then dissociate to unfolded monomers. Different pathways may be related to different charge distributions [63–65]. All the expanded or unfolded states of the dimer are over-simplified by showing one unfolded state. (**b**) The hypothetical, simplified dissociation pathway of PHB dimer at +21. The dimer also expands or unfolds before dissociation. All the expanded or unfolded states of the dimer are over-simplified by showing one expanded state. The folded monomer is the major fragment

constant across the SID E_{lab} of the experiment, it is likely that producing folded monomer does not require precursor unfolding (Scheme 1a). The precursors may need to expand or unfold to produce the unfolded monomer. Because many unfolded states exist, the details of the unfolded states are not specified for simplification.

In contrast, only a low percentage of unfolded monomer is observed in the fragments from dimer at +21 and the major fragment is the folded monomer (Figure 3b). The expanded or unfolded states of the unfragmented precursor at +21 and at +29 have different CCSs and the dissociation differences of these precursors indicate that the structures are not the same.

In CID, low energy barrier products are observed because the collision energy deposits into the precursor stepwise favoring only lower energy pathways. It is possible that CID could dissociate the PHB dimer with higher acceleration voltages than the 200 V maximum available in the instrument, however, higher energy CID requires additional specialized instrument modifications [66]. Supercharging provides another possibility to dissociate the PHB dimer. A previous study has shown that PHB dimer can be supercharged by m-nitrobenzyl alcohol, adding approximately two charge states [67]. Supercharging reagents can sometimes preserve noncovalent protein complex oligomeric state [67, 68]. It is unclear, however, whether supercharging by reagent can always preserve the native structure of protein complexes because data have been reported that some protein complexes unfold [69–72] after supercharging and some do not [8]. Whether CID and SID of supercharged PHB dimer can reflect the native structure is one further direction of this study. SID serves as an alternative activation method to dissociate the refractory PHB dimer without supercharging. In SID, higher energies are deposited into the precursor and high energy barrier fragments are observed. Because of different transmission efficiencies of different *m*/*z* ranges in quadrupole-TOF, the percentages of the species are only semiquantitative. The results for the PHB dimer show one simple application of SID in exploring dissociation pathways for complexes which are resistant to CID within the accessible collision energy of the instrument for the charge states examined.

L-glutamate Dehydrogenase (GDH) Hexamer Dissociates in Surface Induced Dissociation (SID) But Not Significantly in Collision Induced Dissociation (CID)

Bovine GDH is a hexamer of identical 55.6 kDa monomers. The hexamer contains a 3-fold axis and a symmetrical plane perpendicular to the axis [55, 73, 74]. Two odd number charge states (+39 and +27, Supplementary Figure S-5) before and after charge reduction, respectively, of GDH hexamer precursors were selected for dissociation. The hexamer at +39 produced a small amount of monomer (Figure 4a) in the low *m*/*z* region in CID at 200 V (E_{lab} 7800

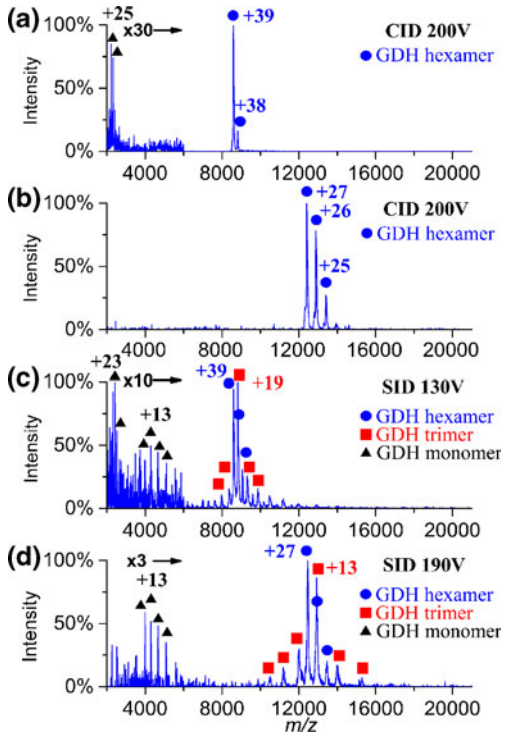

Figure 4. CID and SID spectra of GDH hexamer at +39 and +27. (**a**) GDH hexamer at +39 produces a small amount of highly charged (unfoled) monomer at 200 V acceleration voltage, which is the maximum accessible in the instrument. (**b**) GDH hexamer at +27 does not dissociate significantly in CID at 200 V either but charge stripping peaks are observed at this voltage. (**c**) GDH hexamer at +39 dissociates to a dominant trimer and low abundance monomer at 130 V SID acceleration voltage (5070 eV). The monomer has two charge distributions, one is around +23 and the other is around +13, indicating more than one pathway to form monomer. (**d**) GDH hexamer at +27 dissociates to a dominant trimer and low abundance monomer at 190 V SID acceleration voltage (5130 eV). The E_{lab} of (**c**) and (**d**) are similar, at 5070 and 5130 eV, respectively

eV), which is the maximum CID acceleration voltage accessible in the instrument. This is consistent with a report by the Robinson group showing GDH hexamer (supercharged) produces monomer in CID [32]. No monomer was observed in the 200 V CID spectrum of hexamer at +27 (Figure 4b). Only charge stripping peaks were observed. The accessible E_{lab} of the hexamer at +27 is lower than that at +39 because of voltage limit in the instrument (200 × 27 = 5400 eV vs 200 × 39 = 7800 eV). This may be part of the reason why less fragmentation was observed for the +27 hexamer than for the +39 hexamer. The resistance to dissociation by CID for GDH hexamer shows that this is another refractory complex in the gas phase.

The IM-MS results show that GDH hexamer at +39 unfolds when the CID E_{lab} increases (Supplementary Figure S-6a). The CCS increased to ~200 nm^2 gradually with the E_{lab} increase. The CCS peak width is broader at higher E_{lab} indicating multiple unfolded states exist. CID mainly unfolds the +39 GDH hexamer but does not dissociate it effectively. In contrast to +39, the hexamer at +27 did not unfold in CID but collapsed (Supplementary Figure S-6b), with the CCS decreasing slightly to ~124 nm^2. The CCS peak width is also narrower than that of the +39.

The preference for unfolding of the +39 hexamer probably relates to the mobile protons in the structure. It has been reported that mobile protons can transfer to unfolded parts of protein complex and produce highly charged fragments [27, 28]. Because +27 hexamer has fewer mobile protons, it has less opportunity for protons to transfer to produce an unfolded part, making the energy barrier of the collapse pathway lower than the unfolding pathway. Another possibility is that the conformation of the hexamer varies from +39 to +27, and the energy curves of these two charge states are different, so the lowest energy barrier pathways are different. Nonetheless, CID itself provides limited information for the comparison of the charge states because neither dissociates significantly in CID in this experiment. It was previously reported that m-nitrobenzyl alcohol can cause slight supercharging (average charge increased by 5.7 %) for GDH hexamer allowing asymmetric dissociation in CID following the typical CID pattern [32]. SID clearly provides additional information of the quaternary structure that complements supercharging CID, which for highly charged precursor mainly leads to unfolded hexamer at the energies available in this instrument type.

In contrast to CID, SID dissociates GDH hexamer at +39 and +27 to trimer and monomer (Figure 4c and d). The two SID spectra are acquired under acceleration voltages that correspond to similar E_{lab} for direct comparison of the dissociation of different charge states in SID (130 V for +39 and 190 V for +27 for E_{lab} of 5070 eV an 5130 eV, respectively). The major fragment in SID of the hexamer at +39 is trimer. The charge distribution of trimer is centered at around half of the charge number of the precursor. In other words, the trimer is from the typical SID symmetric dissociation pathway [23–26, 34–36]. Based on the X-ray crystal structure of GDH hexamer [55, 73, 74], the hexamer is composed of two trimers that have a helix twist region to stabilize the substructure (trimer). The fact that SID fragmentation produces dominant trimer but not dominant dimer or monomer agrees with the GDH structure, showing the ability of SID to reveal substructure of a refractory protein complex.

Another more minor product from hexamer at +39 is the monomer (Figure 4c), appearing over two charge distributions with one centered at around +23 and the other one centered at around +13, suggesting two fragmentation pathways to form monomer. Low intensity pentamer around +15 was also observed in the spectrum (not labeled in Figure 4c nor d because the signal was too weak) and is complementary to the +23 monomer. The low intensity of precursor is likely due to the lower transmission efficiency for the higher m/z range compared with lower m/z range

under the experimental conditions. When the E_{lab} was higher, the signal of pentamer was higher (Supplementary Figure S-7c–d). The pathway to produce highly charged monomer (around +23) and the complementary pentamer is asymmetric fragmentation, which involves production of highly charged monomer. Thus, it indicates that significant monomer unfolding for GDH hexamer is observed in SID for the +39 hexamer. The monomers around +13 may be from secondary fragmentation of larger fragments including trimer.

Symmetric fragmentation into trimer is also observed in the SID of hexamer at +27 (Figure 4d). SID can thus provide information about substructure that CID cannot access. Different from the hexamer at +39, fragmentation of hexamer at +27 only produces one charge distribution for monomer around +13 (Supplementary Figure S-7g–h). Although the SID spectrum of +27 seems like a charge-reduced edition of that of +39, IM-MS results revealed that they have differences in the CCSs of the products.

The IM-MS results provide the CCSs of different charge states of the GDH monomers and trimers produced in SID (Figure 5). The monomers are unfolded when the charge state is higher than +12 (Figure 5a) and the trimers are unfolded when the charge state is higher than +19 (Figure 5b). SID of the +27 hexamer produces fewer unfolded monomers based on intensities of the different charge states. The calculated monomer CCS is in agreement with a folded monomer CCS (Figure 5a) and the folded trimer CCS is ~9 % smaller than the calculated CCS (Figure 5b). The CCSs of the GDH fragments are typically constant for a given fragment charge state, independent of the charge state of the precursors that produce the fragments. The result is in agreement with previous studies showing that for a given product ion charge state, the CCSs of the fragments are independent of precursor charge states or activation method [38, 39]. If the charge state of the fragment is the same, the CCS is almost the same.

To explore the details of the dissociation pathways of +39 and +27 of GDH hexamer, different SID acceleration voltages were applied. IM-MS was also used to monitor the CCS of the unfragmented precursor and to distinguish folded and unfolded fragments (Figure 6 and Supplementary Figure S-8). The percentages (Figure 6, zoom-in of the low intensity region in Supplementary Figure S-9) are determined with the same method as described in the PHB study (Figure 3). The +39 precursor unfolds slightly when the E_{lab} is higher than 1500 eV but it does not dissociate to a significant extent until E_{lab} is higher than 2000 eV. When E_{lab} is higher than 2000 eV, the precursor further unfolds and begins to dissociate. Folded and unfolded trimers increase more than other fragments from 2000 to 4500 eV, and monomers start to increase more when E_{lab} is higher than 4500 eV. The E_{lab} onset difference indicates that the energy barrier to form trimers is lower than that to form monomers (Figure 6b and Supplementary Figure S-9a). When E_{lab} is above 6000 eV, the percentages of most fragments do not increase significantly, but the folded trimer decreases slightly while the folded monomer around +13 increases correspondingly (Figure 6b and Supplementary Figure S-9a). The trend suggests that the monomer around +13 may be the product of a secondary fragmentation pathway related to the folded trimer.

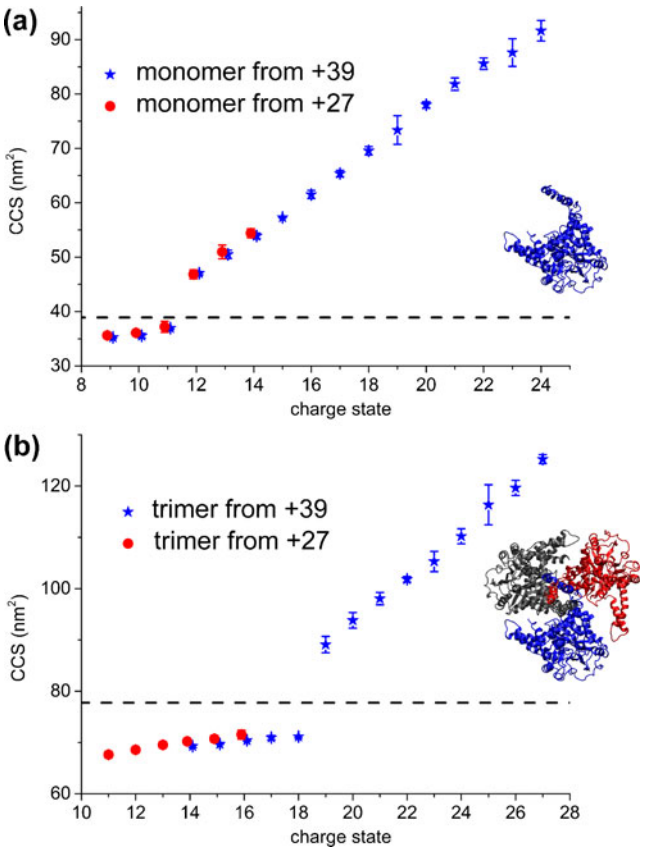

Figure 5. CCSs of different charge states of GDH monomer and trimer in SID. (**a**) CCSs of GDH monomer. Blue filled stars represent CCSs of monomers from GDH hexamer at +39. Red filled circles represent CCSs of monomers from GDH hexamer at +27. The CCSs of +9 to +11 monomers are similar to each other. However, when the charge state is higher than 12, the CCSs increase with charge state shows that higher (≥12) charge state monomers are unfolded to different extents. The dashed line shows the calculated CCS of the GDH monomer clipped from the crystal structure of hexamer. The folded monomer CCSs are only slightly lower (~5 %) than the calculated result. (**b**) CCSs of GDH trimer. Blue filled stars represent CCSs of trimers from GDH hexamer at +39. Red filled circles represent CCSs of trimers from GDH hexamer at +27. The CCSs of +11 to +18 trimers are similar. However, when the charge state is 19 or higher, the CCSs increase with charge state shows that these trimers are unfolded to different extents. The dashed line shows the calculated CCS of the GDH trimer. The folded trimer CCSs are ~9 % smaller than the calculated result. Symbols are slightly displaced to more clearly illustrate overlapping points. The CCSs are measured at three different wave volecities (refer to Experimental) with the range of behavior shown by the error bars

The +27 precursor's CCS decreases slightly when E_{lab} is greater than 810 eV and lower than 2000 eV and begins to increase at E_{lab} 2000 eV (Figure 6c and Supplementary

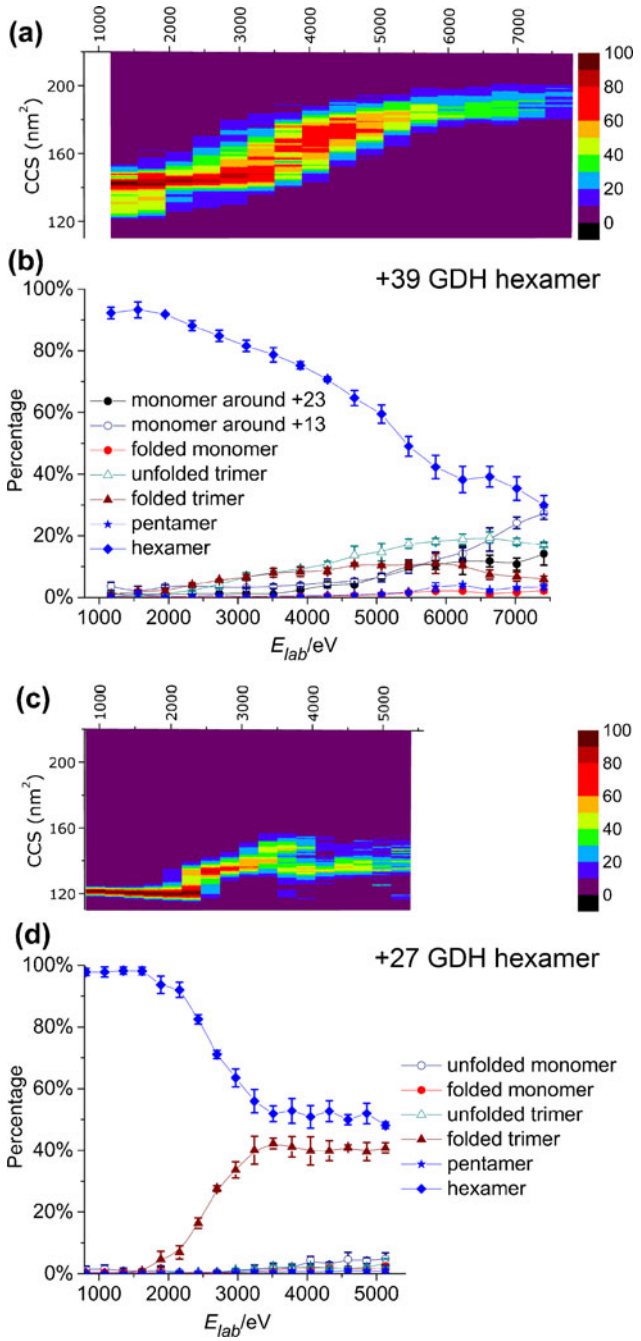

Figure 6. (**a**) Precursor CCSs of GDH hexamer at +39. The intensity is normalized to the percentage of the unfragmented hexamer. The CCS of the unfragmented hexamer increases when E_{lab} increases. (**b**) Percentages of different species formed from +39 precursor. The percentages of the folded and unfolded trimers are similar. (**c**) Precursor CCSs of GDH hexamer at +27. The intensity is normalized to the percentage of the unfragmented hexamer. The CCS of the unfragmented hexamer decreases slightly up to 2000 eV and then increases when E_{lab} is higher than 2000 eV. (**d**) Percentages of different species formed from +27 precursor. Folded trimer is the major fragment across the E_{lab} range. All four plots are aligned in the E_{lab} axis for direct comparison of collision energies. The experiments were performed three times at different wave velocities and wave heights, with the variation of the results marked by the error bars

Figure S-8b). The +27 precursor begins to dissociate when E_{lab} is higher than 2000 eV as well. In contrast to the +39 precursor, the major product from the +27 is the folded trimer. The percentage of the folded trimer stops increasing at 3000 eV and plateaus at higher E_{lab}. The abundances of all the other species are low in the E_{lab} range of this experiment (Figure 6d and Supplementary Figure S-9b). Altough the percentages are not precisely quantitative, the differences of the percentages of the fragments still show that the potential energy surfaces of hexamers at +39 and +27 are qualitatively different. The +39 hexamer has more accessible dissociation pathways than the +27 hexamer, as shown by a wider variety of products. Also, for both charge states, the precursor has to expand or unfold before dissociation, although to a lesser extent for the +27, suggesting the different dissociation pathways have to go through an expanded hexamer. We do not intend to examine the fine details of the dissociation for GDH hexamer from Figure 6b and d because of the added complications from multiple possible pathways in contrast to the simpler dimer system of PHB.

To summarize and explain the observations for SID fragmentation of GDH hexamer at +39 and +27, hypothetical, simplified dissociation pathways are proposed in Scheme 2. IM data show that the +39 precursor is expanded

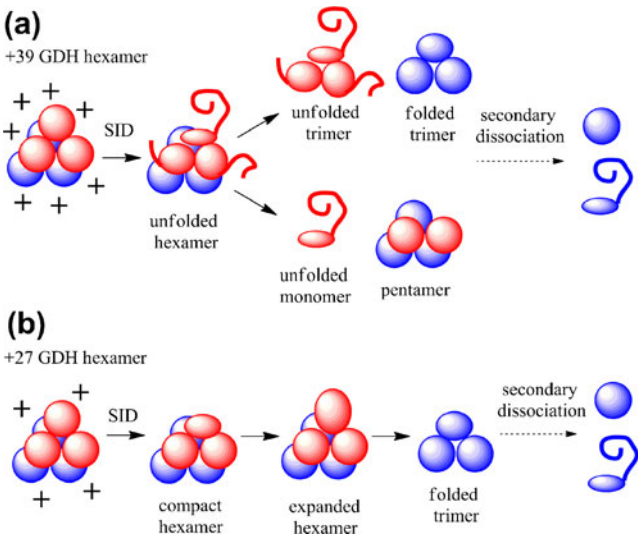

Scheme 2. (**a**) The hypothetical, simplified dissociation pathway of hexamer at +39. All the dissociation pathways are through the partially unfolded hexamer. All the unfolded states of the hexamer are simplified as one unfolded state. Two major dissociation pathways exist. One produces folded and unfolded trimer, the other one forms unfolded monomer and pentamer. (**b**) The hypothetical, simplified dissociation pathway of GDH hexamer at +27. The precursor collapses slightly first and then expands or unfolds slightly. All the compact states of the hexamer are simplified as one state and all the expanded or unfolded states are simplified as one expanded state. Producing the folded trimer is the major dissociation pathway of the +27 precursor. Different colors are used to better distinguish the two trimers. Precursors at both charge states may have secondary dissociation to produce monomers

or unfolded by 25 % before dissociation (Figure 6a and Supplementary Figure S-8a), indicating the unfolding of hexamer is the first step in the dissociation pathway (Scheme 2a). The different unfolded states of the hexamer are not specified because the CCS resolution of the IM is limited, making it difficult to distinguish distinct unfolded states in this case. The unfolded hexamer forms both folded and unfolded trimers, suggesting structural asymmetry of the activated +39 hexamer. Trimers may produce secondary fragments but the intensities of the secondary fragments are too low in the accessible E_{lab} range of SID. Because the secondary dissociation is complicated, they are not specified in Scheme 2 for simplification.

The +27 precursor collapses slightly (Figure 6c and Supplementary Figure S-8b) when the E_{lab} increases, and then expands or unfolds to dissociate (Figure 6c–d and Supplementary Figure S-9b). All compact states are simplified as one state and all unfolded states are simplified as one state in Scheme 2. The major fragment of +27 hexamer is the folded trimer, suggesting the energy barriers to form other fragments are too high to be explored under the experimental conditions. Again, the hexamers with different charge states show distinct dissociation pathways, and the underlying mechanism for the differences is likely a result of the charges but the details are still unclear.

SID shows its ability to reveal substructure information and explore the high energy dissociation pathways of refractory noncovalent protein complexes such as PHB and GDH. After charge reduction using TEAA, more compact products are produced, showing that TEAA can help to preserve native-like conformation of protein complexes.

Conclusion

The success of SID in dissociating PHB dimer and GDH hexamer at different charge states shows the advantages of SID in studying these refractory noncovalent protein complexes. When the energy barrier to dissociation is too high, in spite of significant unfolding, multistep, low target mass CID may not deposit enough energy to overcome the barrier within the voltage limit of the current instrumentation; thus, only precursor unfolding is observed. Therefore, higher energy CID, supercharging, or an alternative activation method is required. In this case, SID provides an alternative solution for dissociation of the complex and for providing quaternary structural information as shown by the data for PHB dimer and GDH hexamer and for GroEL as presented in a recent publication [40]. Supercharging of PHB dimer and GDH hexamer is one possible future direction to dissociate the complexes, although preliminary trials with the reagent m-nitrobenzyl alcohol have not been very efficient in adding charge to either of the proteins, in our lab or as reported in the literature [32, 67]. This study also shows that SID can produce both folded and unfolded products for the two complexes. In GDH, symmetric dissociation and asymmetric dissociation products are observed simultaneously, especially from the +39 hexamer. The precursor charge state determines which dissociation pathway is more prevalent. In both PHB and GDH, precursors at lower charge states generate more folded products and results indicative of native topology. In GDH, the lower charge state yields a symmetric dissociation pathway and folded products more than the higher charge state does. All the results indicate that the lower charge states generate more folded fragments. Based on these experiments, the combination of SID and charge reduction is, thus, a powerful tool for quaternary structure studies of refractory protein complexes that cannot be dissociated by CID.

Acknowledgments

The authors thank Ran An and Jing Yan for their assistance in the experimental work and Yun Zhang for fruitful discussions. This work was financially supported by NSF Grant 0923551 (to VHW). We are grateful for the University of Arizona Research Computing: High Performance Computing/High Throughput Computing Service, which provided computer time for the CCS calculations.

References

1. Loo, J.A.: Studying noncovalent protein complexes by electrospray ionization mass spectrometry. Mass Spectrom. Rev. **16**, 1–23 (1997)
2. Hernandez, H., Robinson, C.V.: Determining the stoichiometry and interactions of macromolecular assemblies from mass spectrometry. Nat. Protoc. **2**, 715–726 (2007)
3. Benesch, J.L., Ruotolo, B.T., Simmons, D.A., Robinson, C.V.: Protein complexes in the gas phase: technology for structural genomics and proteomics. Chem. Rev. **107**, 3544–3567 (2007)
4. Kaddis, C.S., Loo, J.A.: Native protein MS and ion mobility large flying proteins with ESI. Anal. Chem. **79**, 1778–1784 (2007)
5. Heck, A.J.: Native mass spectrometry: a bridge between interactomics and structural biology. Nat. Methods **5**, 927–933 (2008)
6. Heck, A.J., Van Den Heuvel, R.H.: Investigation of intact protein complexes by mass spectrometry. Mass Spectrom. Rev. **23**, 368–389 (2004)
7. Pace, C.N., Trevino, S., Prabhakaran, E., Scholtz, J.M.: Protein structure, stability and solubility in water and other solvents. Philos. Trans. R. Soc. Lond. B Biol. Sci. **359**, 1225–1235 (2004)
8. Hall, Z., Robinson, C.V.: Do charge state signatures guarantee protein conformations? J. Am. Soc. Mass Spectrom. **23**, 1161–1168 (2012)
9. Uetrecht, C., Watts, N.R., Stahl, S.J., Wingfield, P.T., Steven, A.C., Heck, A.J.: Subunit exchange rates in Hepatitis B virus capsids are geometry- and temperature-dependent. Phys. Chem. Chem. Phys. **12**, 13368–13371 (2010)
10. Shoemaker, G.K., van Duijn, E., Crawford, S.E., Uetrecht, C., Baclayon, M., Roos, W.H., Wuite, G.J., Estes, M.K., Prasad, B.V., Heck, A.J.: Norwalk virus assembly and stability monitored by mass spectrometry. Mol. Cell. Proteomics **9**, 1742–1751 (2010)
11. Uetrecht, C., Barbu, I.M., Shoemaker, G.K., van Duijn, E., Heck, A.J.: Interrogating viral capsid assembly with ion mobility-mass spectrometry. Nat. Chem. **3**, 126–132 (2011)
12. Uetrecht, C., Heck, A.J.: Modern biomolecular mass spectrometry and its role in studying virus structure, dynamics, and assembly. Angew. Chem. Int. Ed. **50**, 8248–8262 (2011)
13. Ruotolo, B.T., Benesch, J.L., Sandercock, A.M., Hyung, S.J., Robinson, C.V.: Ion mobility-mass spectrometry analysis of large protein complexes. Nat. Protoc. **3**, 1139–1152 (2008)

14. Uetrecht, C., Rose, R.J., van Duijn, E., Lorenzen, K., Heck, A.J.: Ion mobility mass spectrometry of proteins and protein assemblies. Chem. Soc. Rev. **39**, 1633–1655 (2010)
15. Jurneczko, E., Barran, P.E.: How useful is ion mobility mass spectrometry for structural biology? The relationship between protein crystal structures and their collision cross sections in the gas phase. Analyst **136**, 20–28 (2011)
16. Borsdorf, H., Mayer, T., Zarejousheghani, M., Eiceman, G.A.: Recent developments in ion mobility spectrometry. Appl. Spectrosc. Rev. **46**, 472–521 (2011)
17. Borsdorf, H., Eiceman, G.A.: Ion mobility spectrometry: principles and applications. Appl. Spectrosc. Rev. **41**, 323–375 (2006)
18. Politis, A., Park, A.Y., Hyung, S.J., Barsky, D., Ruotolo, B.T., Robinson, C.V.: Integrating ion mobility mass spectrometry with molecular modeling to determine the architecture of multiprotein complexes. PLoS One **5**, e12080 (2010)
19. Scarff, C.A., Thalassinos, K., Hilton, G.R., Scrivens, J.H.: Traveling wave ion mobility mass spectrometry studies of protein structure: biological significance and comparison with X-ray crystallography and nuclear magnetic resonance spectroscopy measurements. Rapid Commun. Mass Spectrom. **22**, 3297–3304 (2008)
20. Geels, R.B.J., van der Vies, S.M., Heck, A.J.R., Heeren, R.M.A.: Electron capture dissociation as structural probe for noncovalent gas-phase protein assemblies. Anal. Chem. **78**, 7191–7196 (2006)
21. Zhang, H., Cui, W., Wen, J., Blankenship, R.E., Gross, M.L.: Native electrospray and electron-capture dissociation FTICR mass spectrometry for top-down studies of protein assemblies. Anal. Chem. **83**, 5598–5606 (2011)
22. Raspopov, S.A., El-Faramawy, A., Thomson, B.A., Siu, K.W.M.: Infrared multiphoton dissociation in quadrupole time-of-flight mass spectrometry: top-down characterization of proteins. Anal. Chem. **78**, 4572–4577 (2006)
23. Fernandez, F.M., Wysocki, V.H., Futrell, J.H., Laskin, J.: Protein identification via surface-induced dissociation in an FT-ICR mass spectrometer and a patchwork sequencing approach. J. Am. Soc. Mass Spectrom. **17**, 700–709 (2006)
24. Wysocki, V.H., Joyce, K.E., Jones, C.M., Beardsley, R.L.: Surface-induced dissociation of small molecules, peptides, and noncovalent protein complexes. J. Am. Soc. Mass Spectrom. **19**, 190–208 (2008)
25. Wysocki, V.H., Jones, C.M., Galhena, A.S., Blackwell, A.E.: Surface-induced dissociation shows potential to be more informative than collision-induced dissociation for structural studies of large systems. J. Am. Soc. Mass Spectrom. **19**, 903–913 (2008)
26. Beardsley, R.L., Jones, C.M., Galhena, A.S., Wysocki, V.H.: Noncovalent protein tetramers and pentamers with "n" charges yield monomers with n/4 and n/5 charges. Anal. Chem. **81**, 1347–1356 (2009)
27. Felitsyn, N., Kitova, E.N., Klassen, J.S.: Thermal decomposition of a gaseous multiprotein complex studied by blackbody infrared radiative dissociation. Investigating the origin of the asymmetric dissociation behavior. Anal. Chem. **73**, 4647–4661 (2001)
28. Jurchen, J.C., Williams, E.R.: Origin of asymmetric charge partitioning in the dissociation of gas-phase protein homodimers. J. Am. Chem. Soc. **125**, 2817–2826 (2003)
29. Boeri Erba, E., Ruotolo, B.T., Barsky, D., Robinson, C.V.: Ion mobility-mass spectrometry reveals the influence of subunit packing and charge on the dissociation of multiprotein complexes. Anal. Chem. **82**, 9702–9710 (2010)
30. Pagel, K., Hyung, S.J., Ruotolo, B.T., Robinson, C.V.: Alternate dissociation pathways identified in charge-reduced protein complex ions. Anal. Chem. **82**, 5363–5372 (2010)
31. Hall, Z., Politis, A., Bush, M.F., Smith, L.J., Robinson, C.V.: Charge-state dependent compaction and dissociation of protein complexes: insights from ion mobility and molecular dynamics. J. Am. Soc. Mass Spectrom. **134**, 3429–3438 (2012)
32. Hall, Z., Hernández, H., Marsh, J.A., Teichmann, S.A., Robinson, C.V.: The role of salt bridges, charge density, and subunit flexibility in determining disassembly routes of protein complexes. Structure **21**, 1325–1337 (2013)
33. Erba, E.B., Ruotolo, B.T., Barsky, D., Robinson, C.V.: Ion mobility-mass spectrometry reveals the influence of subunit packing and charge on the dissociation of multiprotein complexes. Anal. Chem. **82**, 9702–9710 (2010)
34. Jones, C.M., Beardsley, R.L., Galhena, A.S., Dagan, S., Cheng, G., Wysocki, V.H.: Symmetrical gas-phase dissociation of noncovalent protein complexes via surface collisions. J. Am. Chem. Soc. **128**, 15044–15045 (2006)
35. Blackwell, A.E., Dodds, E.D., Bandarian, V., Wysocki, V.H.: Revealing the quaternary structure of a heterogeneous noncovalent protein complex through surface-induced dissociation. Anal. Chem. **83**, 2862–2865 (2011)
36. Dodds, E.D., Blackwell, A.E., Jones, C.M., Holso, K.L., O'Brien, D.J., Cordes, M.H.J., Wysocki, V.H.: Determinants of gas-phase disassembly behavior in homodimeric protein complexes with related yet divergent structures. Anal. Chem. **83**, 3881–3889 (2011)
37. Zhou, M., Huang, C., Wysocki, V.H.: Surface-induced dissociation of ion mobility-separated noncovalent complexes in a quadrupole/time-of-flight mass spectrometer. Anal. Chem. **84**, 6016–6023 (2012)
38. Zhou, M., Dagan, S., Wysocki, V.H.: Protein subunits released by surface collisions of noncovalent complexes: nativelike compact structures revealed by ion mobility mass spectrometry. Angew. Chem. Int. Ed. **51**, 4336–4339 (2012)
39. Zhou, M., Dagan, S., Wysocki, V.H.: Impact of charge state on gas-phase behaviors of noncovalent protein complexes in collision induced dissociation and surface induced dissociation. Analyst **138**, 1353–1362 (2013)
40. Zhou, M., Jones, C.M., Wysocki, V.H.: Dissecting the large noncovalent protein complex GroEL with surface-induced dissociation and ion mobility-mass spectrometry. Anal. Chem. **85**, 8262–8267 (2013)
41. Ruotolo, B.T., Giles, K., Campuzano, I., Sandercock, A.M., Bateman, R.H., Robinson, C.V.: Evidence for macromolecular protein rings in the absence of bulk water. Science **310**, 1658–1661 (2005)
42. Fernandez-Lima, F.A., Blase, R.C., Russell, D.H.: A study of ion-neutral collision cross-section values for low charge states of peptides, proteins, and peptide/protein complexes. Int. J. Mass Spectrom. **298**, 111–118 (2010)
43. Shelimov, K.B., Jarrold, M.F.: Conformations, unfolding, and refolding of apomyoglobin in vacuum: an activation barrier for gas-phase protein folding. J. Am. Chem. Soc. **119**, 2987–2994 (1997)
44. Badman, E.R., Hoaglund-Hyzer, C.S., Clemmer, D.E.: Monitoring structural changes of proteins in an ion trap over approximately 10–200 ms: unfolding transitions in cytochrome *c* ions. Anal. Chem. **73**, 6000–6007 (2001)
45. Giles, K., Pringle, S.D., Worthington, K.R., Little, D., Wildgoose, J.L., Bateman, R.H.: Applications of a traveling wave-based radio-frequency-only stacked ring ion guide. Rapid Commun. Mass Spectrom. **18**, 2401–2414 (2004)
46. Giles, K., Williams, J.P., Campuzano, I.: Enhancements in traveling wave ion mobility resolution. Rapid Commun. Mass Spectrom. **25**, 1559–1566 (2011)
47. Zhong, Y., Hyung, S.J., Ruotolo, B.T.: Characterizing the resolution and accuracy of a second-generation traveling-wave ion mobility separator for biomolecular ions. Analyst **136**, 3534–3541 (2011)
48. Atmanene, C., Petiot-Becard, S., Zeyer, D., Van Dorsselaer, A., Vivat Hannah, V., Sanglier-Cianferani, S.: Exploring key parameters to detect subtle ligand-induced protein conformational changes using traveling wave ion mobility mass spectrometry. Anal. Chem. **84**, 4703–4710 (2012)
49. Bush, M.F., Hall, Z., Giles, K., Hoyes, J., Robinson, C.V., Ruotolo, B.T.: Collision cross sections of proteins and their complexes: a calibration framework and database for gas-phase structural biology. Anal. Chem. **82**, 9557–9565 (2010)
50. Salbo, R., Bush, M.F., Naver, H., Campuzano, I., Robinson, C.V., Pettersson, I., Jorgensen, T.J., Haselmann, K.F.: Traveling-wave ion mobility mass spectrometry of protein complexes: accurate calibrated collision cross-sections of human insulin oligomers. Rapid Commun. Mass Spectrom. **26**, 1181–1193 (2012)
51. Shvartsburg, A.A., Jarrold, M.F.: An exact hard-spheres scattering model for the mobilities of polyatomic ions. Chem. Phys. Lett. **261**, 86–91 (1996)
52. Mesleh, M.F., Hunter, J.M., Shvartsburg, A.A., Schatz, G.C., Jarrold, M.F.: Structural information from ion mobility measurements: effects of the long-range potential. J. Phys. Chem. **100**, 16082–16086 (1996)
53. Benesch, J.L., Ruotolo, B.T.: Mass spectrometry: come of age for structural and dynamical biology. Curr. Opin. Struct. Biol. **21**, 641–649 (2011)
54. Barford, D., Hu, S.H., Johnson, L.N.: Structural mechanism for glycogen phosphorylase control by phosphorylation and AMP. J. Mol. Biol. **218**, 233–260 (1991)

55. Bailey, J., Powell, L., Sinanan, L., Neal, J., Li, M., Smith, T., Bell, E.: A novel mechanism of V-type zinc inhibition of glutamate dehydrogenase results from disruption of subunit interactions necessary for efficient catalysis. FEBS J. **278**, 3140–3151 (2011)
56. Titani, K., Koide, A., Hermann, J., Ericsson, L.H., Kumar, S., Wade, R.D., Walsh, K.A., Neurath, H., Fischer, E.H.: Complete amino acid sequence of rabbit muscle glycogen phosphorylase. Proc. Natl. Acad. Sci. U. S. A. **74**, 4762–4766 (1977)
57. Nakano, K., Hwang, P.K., Fletterick, R.J.: Complete cDNA sequence for rabbit muscle glycogen phosphorylase. FEBS Lett. **204**, 283–287 (1986)
58. Fletterick, R.J., Madsen, N.B.: The structures and related functions of phosphorylase a. Annu. Rev. Biochem. **49**, 31–61 (1980)
59. Sprang, S.R., Withers, S.G., Goldsmith, E.J., Fletterick, R.J., Madsen, N.B.: Structural basis for the activation of glycogen phosphorylase b by adenosine monophosphate. Science **254**, 1367–1371 (1991)
60. Johnson, L.N., Snape, P., Martin, J.L., Acharya, K.R., Barford, D., Oikonomakos, N.G.: Crystallographic binding studies on the allosteric inhibitor glucose-6-phosphate to T state glycogen phosphorylase b. J. Mol. Biol. **232**, 253–267 (1993)
61. Newgard, C.B., Hwang, P.K., Fletterick, R.J.: The family of glycogen phosphorylases: structure and function. Crit. Rev. Biochem. Mol. Biol. **24**, 69–99 (1989)
62. Fegan, S.K., Thachuk, M.: A charge moving algorithm for molecular dynamics simulations of gas-phase proteins. J. Chem. Theory Comput. **9**, 2531–2539 (2013)
63. Wanasundara, S., Thachuk, M.: Theoretical investigations of the dissociation of charged protein complexes in the gas phase. J. Am. Soc. Spectrom. **18**, 2242–2253 (2007)
64. Wanasundara, S.N., Thachuk, M.: Free energy barrier estimation for the dissociation of charged protein complexes in the gas phase. J. Phys. Chem. A **113**, 3814–3821 (2009)
65. Wanasundara, S.N., Thachuk, M.: Toward an improved understanding of the dissociation mechanism of gas phase protein complexes. J. Phys. Chem. B **114**, 11646–11653 (2010)
66. Benesch, J.L.P., Ruotolo, B.T., Sobott, F., Wildgoose, J., Gilbert, A., Bateman, R., Robinson, C.V.: Quadrupole-time-of-flight mass spectrometer modified for higher-energy dissociation reduces protein assemblies to peptide fragments. Anal. Chem. **81**, 1270–1274 (2008)
67. Lomeli, S.H., Yin, S., Ogorzalek Loo, R.R., Loo, J.A.: Increasing charge while preserving noncovalent protein complexes for ESI-MS. J. Am. Soc. Mass Spectrom. **20**, 593–596 (2009)
68. Lomeli, S.H., Peng, I.X., Yin, S., Ogorzalek Loo, R.R., Loo, J.A.: New reagents for increasing ESI multiple charging of proteins and protein complexes. J. Am. Soc. Mass Spectrom. **21**, 127–131 (2010)
69. Sterling, H.J., Williams, E.R.: Origin of supercharging in electrospray ionization of noncovalent complexes from aqueous solution. J. Am. Soc. Mass Spectrom. **20**, 1933–1943 (2009)
70. Sterling, H.J., Daly, M.P., Feld, G.K., Thoren, K.L., Kintzer, A.F., Krantz, B.A., Williams, E.R.: Effects of supercharging reagents on noncovalent complex structure in electrospray ionization from aqueous solutions. J. Am. Soc. Mass Spectrom. **21**, 1762–1774 (2010)
71. Sterling, H.J., Cassou, C.A., Trnka, M.J., Burlingame, A.L., Krantz, B.A., Williams, E.R.: The role of conformational flexibility on protein supercharging in native electrospray ionization. Phys. Chem. Chem. Phys. **13**, 18288–18296 (2011)
72. Sterling, H., Kintzer, A., Feld, G., Cassou, C., Krantz, B., Williams, E.: Supercharging protein complexes from aqueous solution disrupts their native conformations. J. Am. Soc. Mass Spectrom. **23**, 191–200 (2012)
73. Peterson, P.E., Smith, T.J.: The structure of bovine glutamate dehydrogenase provides insights into the mechanism of allostery. Structure **7**, 769–782 (1999)
74. Smith, T.J., Peterson, P.E., Schmidt, T., Fang, J., Stanley, C.A.: Structures of bovine glutamate dehydrogenase complexes elucidate the mechanism of purine regulation. J. Mol. Biol. **307**, 707–720 (2001)